Circuits Syst Signal Process (2018) 37:3136–3153
https://doi.org/10.1007/s00034-018-0825-5

Exploiting Temporal Correlation for Detection of Non-stationary Signals Using a De-chirping Method Based on Time–Frequency Analysis

Nabeel Ali Khan[1] · **Sadiq Ali**[2]

Received: 15 August 2017 / Revised: 14 April 2018 / Accepted: 23 April 2018 /
Published online: 3 May 2018

Abstract Novel time–frequency ($t-f$) methods are developed for the detection of non-stationary signals in the presence of noise with uncertain power. The proposed method uses instantaneous frequency estimation and de-chirping procedure to convert a non-stationary signal into a stationary signal, thus allowing us to exploit temporal correlation as an extra feature for signal detection in addition to the signal energy. The proposed method can be used for both mono-sensor and multi-sensor recordings. Area under receiver operating characteristic curve and probability of signal detection are used as criteria for comparing the performance of the proposed signal detection methods with the state of the art in the presence of noise power uncertainty. Simulation results indicate the superiority of the proposed approach.

Keywords Non-stationary signal detection · De-chirping · Instantaneous frequency · Temporal correlation

1 Introduction

Frequency-modulated signals also known as chirp signals are frequently observed in nature. Bats and dolphins use chirp signals for locating food and navigating in the skies or oceans [23]. Similarly, in order to communicate with each other, whales use

✉ Nabeel Ali Khan
nabeel.alikhan@gmail.com

Sadiq Ali
dr.sadiq.ali.turi@gmail.com

1 Electrical Engineering, Foundation University, Islamabad, Pakistan

2 Department of Electrical Engineering, University of Engineering and Technology, Peshawar, Pakistan

chirp-like signals to sing long and complex songs. In radar, sonar and remote sensing, chirp signals are used to navigate and detect the desired targets [14]. In communication systems, information can be transmitted using chirps, where transmitter encodes the information by phase and frequency modulations. In astrophysics, gravitational waves that emerge due to the disturbances in the curvature of space–time also posses chirp-like characteristics [5]. Chirp signals are also used for jamming in electronic warfare because of their wideband characteristics.

Detection of weak chirp signals in a very noisy environment is important for many military and commercial applications [5]. Commonly used methods for signal detection include energy detector, matched filter and detectors exploiting cyclostationarity [6,30,31]. The performance of these methods depends on the use of available prior knowledge about signals. For example, if the signal is known to the receiver, matched filter is an optimal detector [3]. Energy detector on the other hand does not require knowledge about the signal, but requires the noise power to be known [30,31]. Energy detector performs very poorly in the case of noise uncertainty as, in practice, obtaining accurate estimates of noise powers is not possible [2,21,25,25,26]. Hence, there is a need of completely blind detection schemes that require very little or no prior information about signal and noise [3,6,30,31].

In many practical cases received signals are correlated in space or time due to the presence of spatially or temporally correlated channels oversampling at the receiver, or because of the inherent characteristics of a transmitted signal [28,32]. In order to achieve better detection performances, extra features such as spatial or temporal correlation could be exploited in addition to signal energy [2,3]. These correlations can be considered as side information that can also be used to bring robustness to the detection process against noise power uncertainty [2,3,31]. However, these methods are used for stationary signals and are expected to under-perform for non-stationary signals.

Time–frequency distributions (TFDs) are powerful tools for the analysis of non-stationary FM signals. TFDs concentrate energy of such non-stationary signals along their instantaneous frequencies while spreading the noise in entire $t-f$ plane. One commonly used $t-f$ signal detection approach is to employ matched filtering or correlation [20]. A given signal is transformed in the $t-f$ domain and then correlated with a set of predetermined templates. These methods have been successfully applied for the detection of seizures in newborns [20]. Experimental results have shown that $t-f$ matched filtering can outperform conventional time-domain matched filter in case of non-Gaussian noise [20]. However, effective implementation of these methods requires prior information regarding the nature of underlying signal to prepare templates [9]. For example, in case of EEG signals piecewise linear frequency modulation characteristics of the seizure signals are exploited for preparing templates [9]. Similarly, signal energy concentrated along the instantaneous frequency (IF) of a frequency-modulated signal can be used as a test statistic for the detection of non-stationary signals [22]. This method does not require any prior information regarding the IF structure of the given signal.

The aforementioned $t-f$-based detection methods either assume known signals, or only exploit signal energy along IF curves for signal detection and fail to exploit

spatial or temporal correlation in slowly changing amplitudes of signal components. In this study, we develop a new completely blind scheme for signal detection that:

1. is completely blind and does not require prior information regarding the structure of the desired signal.
2. assumes no knowledge about the noise and performs well even when noise power is unknown. Therefore, the proposed scheme is robust against the noise power uncertainty.
3. is equally applicable to both mono-sensor and multi-sensor recordings.

In order to achieve the above goals, the proposed detection scheme uses TFD to estimate IF estimation, which is then employed to de-chirp the given signal. The de-chirping results in a temporally correlated stationary version of a non-stationary signal. This inherent correlation is then exploited using covariance matrix-based approach for signal detection in both mono-sensor and multi-sensor recordings.

Experimental results indicate the superiority of the proposed method as compared to conventional time-domain approaches while considering a challenging scenario when noise power is uncertain.

2 Time–Frequency Mono-sensor Detector

2.1 Signal and System Model

In this section we consider a receiver with a single sensor that receives N samples of the desired signals in the presence of additive white Gaussian noise (AWGN) with uncertain noise power [25]. These N observed samples are stacked in a $N \times 1$ vector $\mathbf{x}$, and the detection model for the received signal can be described as:

$$\begin{aligned} \mathcal{H}_1 &: \mathbf{x} = \mathbf{s} + \mathbf{w} \\ \mathcal{H}_0 &: \mathbf{x} = \mathbf{w}, \end{aligned} \tag{1}$$

where $\mathbf{s} = [s[1], s[2], \ldots, s[N]]$ with $s(n) = a(n)\exp(j\varphi(n))$ being the nth sample of noise-free desired signal, in which $\varphi(n)$ is the instantaneous phase and $a(n)$ is the slowly varying instantaneous amplitude whose spectrum does not overlap with the spectrum of $e^{j\varphi(n)}$. With this received signal model, the goal is to design robust detection scheme against noise power uncertainty.

2.2 Proposed Detection Scheme

Existing covariance-based approaches [1,3,4,30] are blind and assume no a priori knowledge. They are robust against the noise power uncertainty as they instantly estimate noise powers. However, these methods exploit temporal correlation assuming that the given signal is stationary. The aim of this work is to extend the aforementioned detector for frequency-modulated signals. The aforementioned model of FM signals indicate that instantaneous amplitude of such signals is correlated in time, while non-stationarity is caused by $e^{j\varphi(n)}$. In the following section, a t–f approach

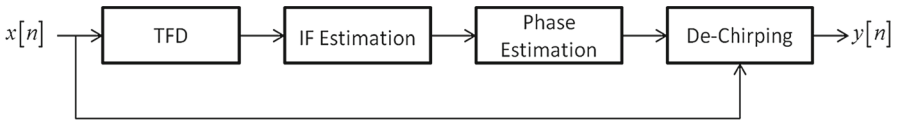

Fig. 1 Steps for stationarization of the received signals at mono-sensor receiver

will be developed to stationarize the received signal by first estimating the instantaneous frequency and then using it to stationarize the received signal. For the case of non-stationary process, the proposed scheme that exploits both t–f techniques and temporal correlation is described in the following subsections and illustrated in Fig. 1.

2.2.1 Computation of Time–Frequency Distribution

A TFD of a received signal $\{x\,(n)\}_{n=1}^{N}$ is computed as:

$$\rho\,[n,k] = \sum_{m} G\,[n,m] \underset{n}{*} x\,[n+m]\,x^{*}\,[n-m]\,e^{-\frac{j2\pi mk}{N}}, \tag{2}$$

where n is time index, k is frequency bin, N is total number of time-domain samples, and $G\,[n,m]$ is a time-lag kernel. In this study, we have selected modified B distribution (MBD) though we can employ other sophisticated methods such as locally adaptive directional TFDs to improve robustness against noise [7,10,15,19]. The selected time-lag kernel is defined as:

$$G[n,m] = \frac{\cosh^{-2\beta}[n]}{\sum_i \cosh^{-2\beta}[i]}, \tag{3}$$

where $\beta = 0.2$ in this study.

2.2.2 Instantaneous Frequency and Phase Estimation

After having clear TFD $\rho\,[n,k]$ of the received signals, we estimate the instantaneous frequency of the signal by detecting the location of the peak frequency at each time instant as:

$$\hat{f}\,[n] = \arg\max_{k} \rho\,[n,k]\,. \tag{4}$$

Note that we can employ sophisticated methods such as random sample consensus (RANSAC) and Viterbi-based algorithms to obtain accurate estimate of the instantaneous frequency [12,24]. For continuous time signals, the instantaneous phase, i.e., $\varphi(t)$, is related to instantaneous frequency, i.e., $f\,(t)$, by the integral operation [8].

$$\varphi\,(t) = \int_{0}^{t} f(\tau)\mathrm{d}\tau. \tag{5}$$

In case of discrete signals, the instantaneous phase of the signal is estimated using the following operation:

$$\hat{\varphi}[n] = \hat{\varphi}[n-1] + \frac{2\pi}{N}\hat{f}[n], \tag{6}$$

where N is the total number of frequency bins in a TFD. Note that the above-mentioned expression can estimate phase up to a constant as initial phase is not known and assumed to be zero, i.e., $\hat{\varphi}[n] = 0$.

2.2.3 Time–Frequency Filtering (De-chirping)

Once we have the estimate of instantaneous phase, the next step is to de-chirp the given signal using the estimated phase. The de-chirping operation converts a non-stationary signal into a stationary signal by removing the frequency modulation. The de-chirping operation has found widespread applications in non-stationary signal processing, such as component extraction, signal analysis, parameter estimation, instantaneous frequency estimation [11,13,18,27]. In case of a multi-component signal, the strongest component is converted into DC or stationary signal. The process in the case of hypothesis $\mathcal{H}_1$ can be represented as:

$$\begin{aligned} y[n] &= x[n]\exp\left(-j\hat{\varphi}[n]\right) \\ &= s[n]\exp\left(-j\hat{\varphi}[n]\right) + w[n]\exp\left(-j\hat{\varphi}[n]\right) \\ &\approx \alpha\exp\left(-j\left(\hat{\varphi}[n]-\varphi[n]\right)\right) + \tilde{w}[n] \\ &\quad \alpha\exp(-j\phi) + \tilde{w}[n] \\ &\approx \tilde{s}[n] + \tilde{w}[n], \end{aligned} \tag{7}$$

where ϕ is a constant phase. The above equation is based on the assumption that estimated instantaneous phase is approximately equal to original instantaneous phase up to a constant, i.e., $\hat{\varphi}[n] \approx \varphi[n]+\phi$. The above equation illustrates that the de-chirped signal, i.e., $\tilde{s}[n] = \alpha\exp(-j\phi)$, is a constant as it has no time-varying part. Note that this derivation is based on assumption that the observed signal is a frequency-modulated signal, i.e., $s[n] = \alpha\exp(-j\varphi[n])$, with no variations in instantaneous amplitude. Such signals are frequently encountered in radars. The t–f signature of such de-chirped signals is a straight line parallel to the time axis in the t–f plane [29], e.g., Fig. 2 illustrates how t–f representation of a non-stationary signal changes when it is stationarized by de-chirping.

The uncorrelated white Gaussian noise remains uncorrelated with the same power even after de-chirping, i.e.,

$$E[\tilde{w}^*[n]\tilde{w}[n+l]] = e^{j2\pi(\theta(n+l)-\theta(n))}E[w^*[n]w[n+l]] = \sigma^2\delta(l). \tag{8}$$

Now the $N \times 1$ vector $\mathbf{y} = [y[1], y[2], \ldots, y[N]]^{\mathrm{T}}$ contains stationary version of non-stationary signals in vector $\mathbf{x}$. The detection problem becomes

$$\begin{aligned} \mathcal{H}_1 &: \mathbf{y} = \tilde{\mathbf{s}} + \tilde{\mathbf{w}} \\ \mathcal{H}_0 &: \mathbf{y} = \tilde{\mathbf{w}}, \end{aligned} \tag{9}$$

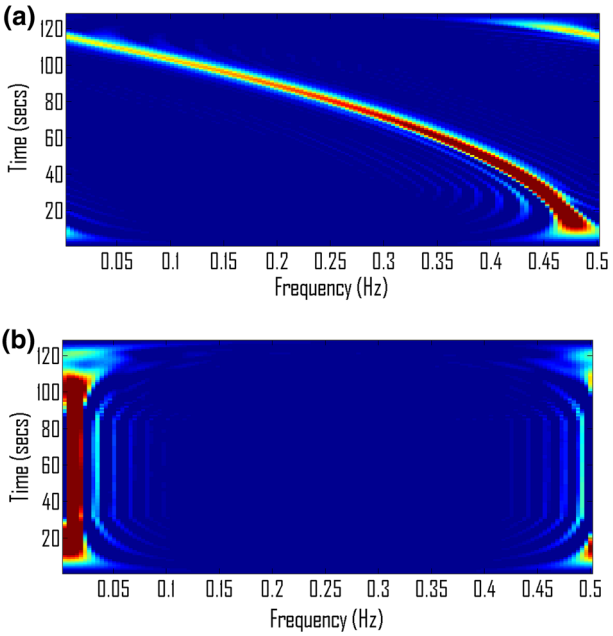

Fig. 2 Transformation of a non-stationary frequency-modulated signal into a stationary signal by de-chirping. **a** Time–frequency representation of non-stationary quadratic chirp. **b** Time–frequency representation of a stationarized signal

where $\tilde{\mathbf{s}} = \left[\tilde{s}\,[1], \tilde{s}\,[2], \ldots, \tilde{s}\,[N]\right]$ and $\tilde{\mathbf{w}} = \left[\tilde{w}\,[1], \tilde{w}\,[2], \ldots, \tilde{w}\,[N]\right]$. The covariance matrices of $\mathbf{y}$ and $\tilde{\mathbf{s}}$ are given as:

$$\begin{aligned}\boldsymbol{\Sigma}_{\mathbf{y}} &= \mathrm{E}[\mathbf{y}(n)\mathbf{y}^{\mathrm{T}}(n)]\\ \boldsymbol{\Sigma}_{\mathbf{s}} &= \mathrm{E}[\tilde{\mathbf{s}}(n)\tilde{\mathbf{s}}^{\mathrm{T}}(n)]\\ \boldsymbol{\Sigma}_{\mathbf{w}} &= \mathrm{E}[\tilde{\mathbf{w}}(n)\tilde{\mathbf{w}}^{\mathrm{T}}(n)].\end{aligned}$$

These two covariance matrices $\boldsymbol{\Sigma}_{\mathbf{y}}$ and $\boldsymbol{\Sigma}_{\mathbf{s}}$ can be related as:

$$\boldsymbol{\Sigma}_{\mathbf{y}} = \boldsymbol{\Sigma}_{\mathbf{s}} + \boldsymbol{\Sigma}_{\mathbf{w}}, \tag{10}$$

where $\boldsymbol{\Sigma}_{\mathbf{w}} = \sigma^2\mathbf{I}$ as noise remains uncorrelated even after de-chirping. Off-diagonal elements of signal covariance matrix $\boldsymbol{\Sigma}_{\mathbf{s}}$ capture temporal correlation between signals that can be exploited as side information to detect the presence of the desired signal in the observed signals. Exploiting the temporal correlation using covariance matrix as a priori information can effectively circumvent the problem against the noise power uncertainty faced by the traditional energy-based detection mechanisms.

2.2.4 Generalized Likelihood Ratio Test

The obtained signals, $\mathbf{y} = [y[1], y[2], \ldots, y[N]]^{\mathrm{T}}$, posses temporal correlation. In order to exploit the temporal correlation jointly with the energy of the signals, we need to solve the following generalized likelihood ratio test (GLRT) equation [4]:

$$\Lambda[\mathbf{y}] = \frac{\max\limits_{\boldsymbol{\Sigma}_{1,\mathbf{y}}} f\left(\mathbf{y}; \boldsymbol{\Sigma}_{1,\mathbf{y}}\right)}{\max\limits_{\boldsymbol{\Sigma}_{0,y}} f\left(\mathbf{y}; \boldsymbol{\Sigma}_{0,\mathbf{y}}\right)} \underset{\mathcal{H}_0}{\overset{\mathcal{H}_1}{\gtrless}} \lambda, \tag{11}$$

where $f\left(\mathbf{y}; \boldsymbol{\Sigma}_{1,\mathbf{y}}\right)$ and $f\left(\mathbf{y}; \boldsymbol{\Sigma}_{0,\mathbf{y}}\right)$ are the probability distributions (likelihood functions) with $\boldsymbol{\Sigma}_{1,\mathbf{y}}$ and $\boldsymbol{\Sigma}_{0,\mathbf{y}}$ exhibiting temporal correlation present in $\mathbf{y}$ under hypothesis $\mathcal{H}_1$ and $\mathcal{H}_0$, respectively. In (11), $\max\limits_{\boldsymbol{\Sigma}_{1,\mathbf{y}}} f\left(\mathbf{y}; \boldsymbol{\Sigma}_{1,\mathbf{y}}\right)$ and $\max\limits_{\boldsymbol{\Sigma}_{0,\mathbf{y}}} f\left(\mathbf{y}; \boldsymbol{\Sigma}_{0,\mathbf{y}}\right)$ are maximum likelihood estimation-based solutions under hypothesis $\mathcal{H}_1$ and $\mathcal{H}_0$, respectively. Solving (11), we get

$$\ell[\mathbf{y}] = \frac{\det \hat{\boldsymbol{\Sigma}}_{1,\mathbf{y}}}{\det \hat{\boldsymbol{\Sigma}}_{0,\mathbf{y}}} \underset{\mathcal{H}_0}{\overset{\mathcal{H}_1}{\gtrless}} \lambda_1, \tag{12}$$

where det is short for determinate, $\hat{\boldsymbol{\Sigma}}_{1,\mathbf{y}} = \mathrm{E}\left[\mathbf{y}\mathbf{y}^H\right]$, and $\hat{\boldsymbol{\Sigma}}_{0,\mathbf{y}} \approx \mathrm{diag}\,\hat{\boldsymbol{\Sigma}}_{1,\mathbf{y}}$ [3]. The traditional GLRT scheme would be similar to (12) but replacing $\hat{\boldsymbol{\Sigma}}_{1,\mathbf{y}}$ with $\hat{\boldsymbol{\Sigma}}_{1,\mathbf{x}} = \mathrm{E}\left[\mathbf{x}\mathbf{x}^H\right]$ in (11). It is to be noted that $\mathbf{x}$ is the preprocessed version of $\mathbf{y}$. We further remark that GLRT is asymptotically an optimal detection method [2].

2.2.5 Covariance Absolute Value Detector

The covariance absolute value (CAV) detector is a ratio between the sum of absolute value of elements of the sample covariance matrix $\hat{\boldsymbol{\Sigma}}_{1,\mathbf{y}}$ and the sum of diagonal elements of it. Let T_1 be defined as sum of all elements of $\hat{\boldsymbol{\Sigma}}_{1,\mathbf{y}}$

$$T_1(\mathbf{y}) = \sum_{n=1}^{N}\sum_{m=1}^{N} \mathrm{abs}(\lambda_{nm}), \tag{13}$$

where λ_{nm} represents the elements of covariance matrix. Let T_2 be defined as sum of all elements of $\hat{\boldsymbol{\Sigma}}_{0,\mathbf{y}}$.

$$T_2(\mathbf{y}) = \sum_{n=1}^{N} \mathrm{abs}(\lambda_{nn}). \tag{14}$$

If signal is not present, i.e., $\boldsymbol{\Sigma}_{\mathbf{s}} = 0$, then all off-diagonal elements of $\boldsymbol{\Sigma}_{\mathbf{y}}$ become equal to zero. In such scenario, sum of all elements of $\boldsymbol{\Sigma}_{\mathbf{y}}$ would be equal to sum of its diagonal elements, i.e., $T_1 = T_2$ [31]. In case if signal is present then all off-diagonal elements of $\boldsymbol{\Sigma}_{\mathbf{y}}$ would be nonzero, which will make $T_1 > T_2$ [31]. This implies we can use the following test static for signal detection.

$$T(\mathbf{y}) = \frac{T_1(\mathbf{y})}{T_2(\mathbf{y})} \underset{\mathcal{H}_0}{\overset{\mathcal{H}_1}{\gtrless}} \gamma. \tag{15}$$

The traditional CAV detector scheme is similar to the proposed methods expressed in Eq. (15). For original time-domain detector, the covariance matrix is estimated from original time-domain signal, whereas the proposed method uses de-chirped signal, i.e., $\hat{\boldsymbol{\Sigma}}_{1,\mathbf{y}}$ has replaced $\hat{\boldsymbol{\Sigma}}_{1,\mathbf{x}} = \mathrm{E}\left[\mathbf{x}\mathbf{x}^H\right]$.

2.3 Performance Comparison

Let us consider a non-stationary signal defined as:

$$s = e^{2\pi j(an+bn^3)}, \tag{16}$$

where $a = 0.5$ and $b = 1.2207e-05$. The given signal is corrupted with white Gaussian noise with uncertain noise power. The uncertain noise power is generated as:

$$\sigma_{un}^2 \sim \mathcal{U}\left(\frac{\sigma^2}{\alpha_{nu}}, \alpha_{nu}\sigma^2\right), \tag{17}$$

where $\alpha_{nu} \geq 1$ and $\alpha_{nu} = 1$ means no noise uncertainty [25]. In this study, we have assumed $\alpha_{nu} = 2$. It is to be noted that σ^2 is mean noise power of σ_{un}^2. Such an uncertainty in the noise power knowledge deteriorates the performance of detection schemes. In the presence of such an uncertainty, the performance of the proposed t–f signal detection techniques is compared with original time-domain covariance methods [31], ridge energy detector [22], t–f correlator [20] and energy detector using receiver operating characteristic (ROC) curve analysis, whereas the energy detector is formulated as:

$$T_{\text{Energy}}(\mathbf{x}) = \frac{1}{N}\sum_{n=1}^{N} x^2(n) \underset{\mathcal{H}_0}{\overset{\mathcal{H}_1}{\gtrless}} \gamma. \tag{18}$$

The ROC curve obtained using GLRT and CAV detectors are shown in Figs. 3 and 4, respectively. It can be observed that the proposed schemes perform better than the traditional schemes. Areas under each ROC curve (AUCs) for these two approaches are given in Table 1. Note that the AUC is always between 0.5 (worst) and 1.0 (best). It is because the worst ROC curve lies along the diagonal and it has an area of 0.5. The best ROC curve has an area of 1. All of the above experimental results indicate that the proposed signal detection method outperforms the conventional schemes.

In order to further analyze the proposed schemes in comparison with the traditional schemes we plot the probability of detection at a false alarm rate of 1% versus SNR. These plots are shown in Fig. 5 for GLRT and in Fig. 6 for CAV detectors. Once again we can clearly see that the proposed methods achieve better performance as compared to traditional methods. This improved performance is due to conversion of a non-stationary signal into stationary one by the use of t–f processing thus allowing us to exploit temporal correlation in addition to signal energy. These results are plotted for the noise power uncertainty value $\alpha_{nu} = 2$.

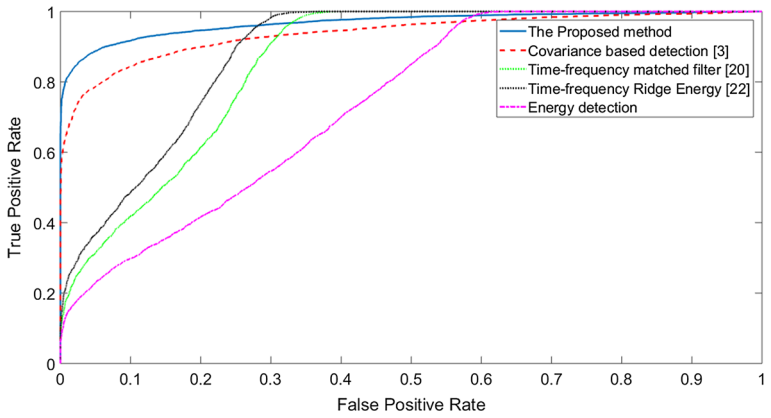

Fig. 3 Performance comparison between $t-f$ generalized likelihood ratio test versus time-domain generalized likelihood test [3,4], $t-f$ ridge detector [22], $t-f$ correlator [20] and energy detector Eq. (18). Noise power uncertainty parameter $\alpha_{nu} = 2$

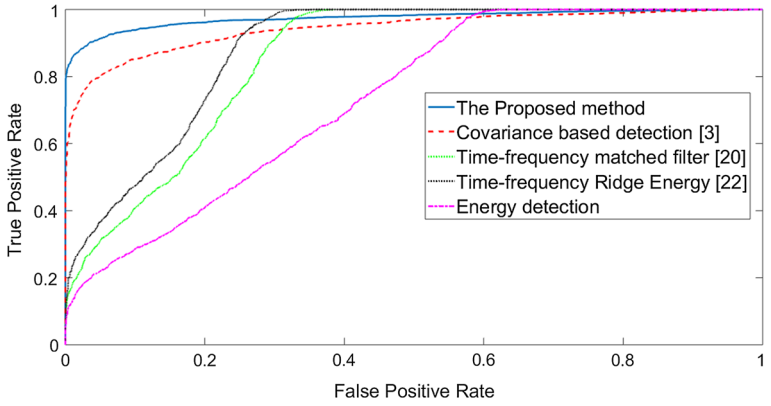

Fig. 4 Performance comparison between $t-f$ covariance absolute value detector versus time-domain covariance absolute value detector [31], $t-f$ ridge detector [22], $t-f$ correlator [20] and energy detector Eq. (18). Noise power uncertainty parameter $\alpha_{nu} = 2$

Table 1 Area under ROC curve of $t-f$ detectors versus conventional detection methods

$t-f$ CAV	CAV [31]	$t-f$ GLRT	GLRT [3]	Energy detector	Ridge energy detector [22]
0.9744	0.9392	0.9701	0.9436	0.7343	0.8856

Noise power uncertainty parameter $\alpha_{nu} = 2$

3 Extension to Multi-sensor Detection Scheme

In this section we consider the multi-sensor detector at the receiver side to exploit the spatial correlation in addition to temporal correlation [3]. Earlier signal detection methods given in [3] assume stationary signals and are expected to under-perform for the detection of non-stationary signals. In this study, we extend these conven-

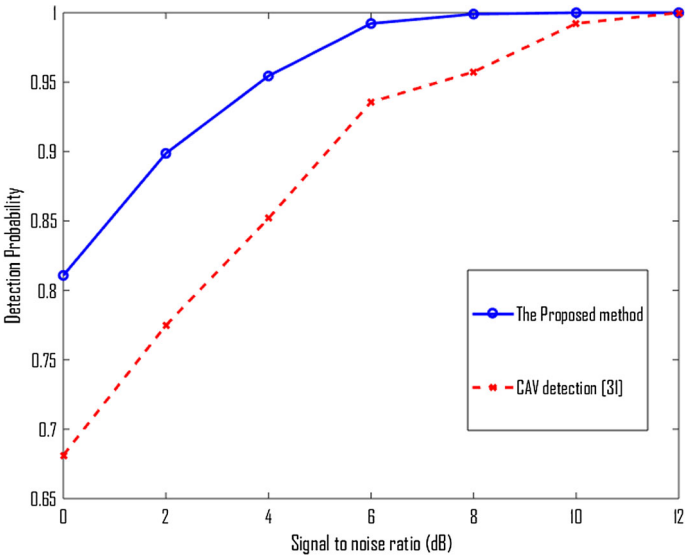

Fig. 5 Performance comparison between $t-f$ GLRT versus traditional GLRT [3,4]. Noise power uncertainty parameter $\alpha_{nu} = 2$

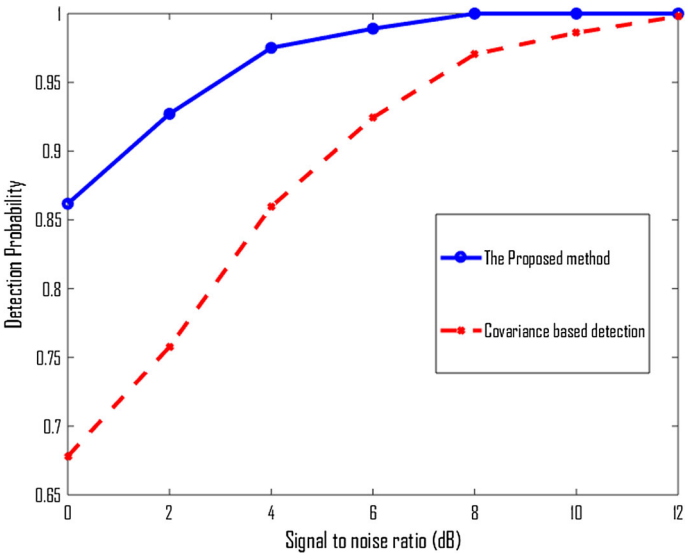

Fig. 6 Performance comparison between $t-f$ CAV detector versus traditional CAV detector [31]. Noise power uncertainty parameter $\alpha_{nu} = 2$

tional multi-sensor signal detection approaches to non-stationary signals by using $t-f$ processing. The proposed multi-sensor schemes are similar to mono-sensor signal detection schemes in a way that the key step of signal stationarization is common in

both methods. However, in order to exploit spatial diversity for multi-sensor recordings, the following additional steps are performed.

- Spatial averaging of TFDs computed at each sensor is performed to overall SNR, thus improving the accuracy of IF estimate.
- Spatiotemporal GLRT and spatiotemporal CAV detectors are employed instead of temporal GLRT and temporal CAV to exploit both spatial diversity and temporal diversity.

3.1 Multi-sensor Signal Model

Lets us assume that M sensors are available to detect the non-stationary signal received from the source. When the signal is present then at the mth sensor, the received signal vector can be represented as: $\mathbf{x}_m = \mathbf{s}_m + \mathbf{w}_m$, whereas in the absence of source signal, we have $\mathbf{x}_m = \mathbf{w}_m$. Hence, the signal model at the mth sensor of the receiver can be written as:

$$\begin{aligned} \mathcal{H}_1 &: \mathbf{x}_m = \mathbf{s}_m + \mathbf{w}_m \\ \mathcal{H}_0 &: \mathbf{x}_m = \mathbf{w}_m, \end{aligned} \tag{19}$$

where $\mathbf{x}_m = [x_m[1], x_m[1], \ldots, x_m[N],]$ contains N samples of the observed signals at the mth sensor, $\mathbf{s}_m = [s_m[1], s_m[1], \ldots, s_m[N],]$ contains noiseless signal, and $\mathbf{w}_m = [w_m[1], w_m[1], \ldots, w_m[N],]$ contains N samples of Gaussian noise.

Now the goal is to exploit both spatial and temporal correlations in the detection process. Therefore, we need to perform the t–f processing to extract the embedded spatiotemporal correlation.

3.2 Time–Frequency Processing

The process of stationarization for multi-sensor detection scheme is illustrated in Fig. 7. Just like in the mono-sensor case, quadratic TFD is computed for the signal acquired at the mth sensor as:

$$\rho_m[n,k] = \sum_l G[n,l] \underset{n}{*} x_m[n+l]\, x_m^*[n-l]\, e^{-\frac{2\pi jlk}{N}}, \tag{20}$$

where $m = 1, 2, \ldots, M$. These TFDs are then spatially averaged as

$$\rho_{\text{avg}}[n,k] = \frac{1}{M} \sum_{m=1}^{M} \rho_m[n,k]. \tag{21}$$

The $\rho_{\text{avg}}[n,k]$ is now a single TFD . Using $\rho_{\text{avg}}[n,k]$, the IF $f(n)$ and phase $\hat{\varphi}(n)$ of the source signal can be estimated following the process given in Sect. 2.2. Once we have the estimate of instantaneous phase, the next step is to de-chirp the given signal using the estimated phase $\hat{\varphi}(n)$. The de-chirping process at the mth sensor in the case

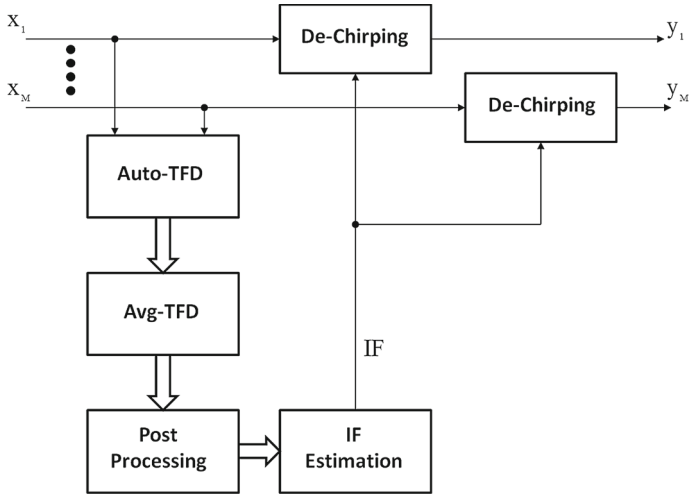

Fig. 7 Illustration of the process of stationarization of the received signals at multi-sensor receiver

of hypothesis $\mathcal{H}_1$ can be represented as:

$$\begin{aligned} y_m[n] &= x_m[n] \exp\left(-j\hat{\varphi}(n)\right) \\ &= \tilde{s}_m[n] + \tilde{w}_m[n]. \end{aligned} \tag{22}$$

The N samples of the stationary version of signals received at M sensors are stacked in $M \times N$ matrix $\mathbf{Y}$ as:

$$\mathbf{Y} = \begin{bmatrix} \mathbf{y}_1 \\ \mathbf{y}_2 \\ \vdots \\ \mathbf{y}_M \end{bmatrix}, \tag{23}$$

where $\mathbf{y}_m = [y_m[1], y_m[1], \ldots, y_m[N],]$ is the stationary version of $\mathbf{x}_m$. By using *vec* operator we find $\mathbf{z} = \text{vec}(\mathbf{Y})$ as:

$$\mathbf{z} = \left[\left[y_1[1]\ y_2[1] \cdots y_M[1] \right], \ldots, \left[y_1[N]\ y_2[N] \ldots y_M[N] \right]\right]^{\mathrm{T}}. \tag{24}$$

The $NM \times 1$ vector $\mathbf{z}$ is used to design detection scheme using spatiotemporal correlation in addition to the energy of the received signals.

3.3 Spatiotemporal GLRT

In this section we exploit the spatiotemporal correlation for the detection problem introduced in Eq. (19) by adopting the GLRT approach given in (11). In this case the GLRT scheme can be formulated as:

$$\Lambda_{\mathrm{ST}}(\mathbf{z}) = \frac{\max\limits_{\boldsymbol{\Sigma}_{z,1}} f_{\mathbf{z}}\left(\mathbf{z};\, \boldsymbol{\Sigma}_{z,1}\right)}{\max\limits_{\boldsymbol{\Sigma}_{z,0}} f_{\mathbf{z}}\left(\mathbf{z};\, \boldsymbol{\Sigma}_{z,0}\right)} \quad \underset{\mathcal{H}_0}{\overset{\mathcal{H}_1}{\gtrless}} \gamma, \tag{25}$$

where $f_{\mathbf{z}}\left(\mathbf{z}, \boldsymbol{\Sigma}_{z,0}\right)$ and $f_{\mathbf{z}}\left(\mathbf{z};\, \boldsymbol{\Sigma}_{z,1}\right)$ are the likelihood functions under hypothesis $\mathcal{H}_0$ and $\mathcal{H}_1$, respectively. Solving (25), we can get the final expression of the GLRT as:

$$\Lambda_{\mathrm{ST}}(\mathbf{z}) = \left| \frac{\hat{\boldsymbol{\Sigma}}_{z,1}}{\hat{\boldsymbol{\Sigma}}_{z,0}} \right| \underset{\mathcal{H}_1}{\overset{\mathcal{H}_0}{\gtrless}} \gamma, \tag{26}$$

where $\hat{\boldsymbol{\Sigma}}_{z,1} = \mathrm{E}\left[\mathbf{z}\mathbf{z}^H\right]$ and $\hat{\boldsymbol{\Sigma}}_{z,0} = \mathrm{diag}\left[\hat{\boldsymbol{\Sigma}}_{z,1}\right]$. Note that the detection scheme in (26) assumes no structure for the covariance matrix, except that the covariance matrix is symmetric.

3.4 Spatiotemporal CAV Detector

In order to use the detection scheme (25), a critical requirement is that the sample covariance matrices $\hat{\boldsymbol{\Sigma}}_{z,1}$ must be non-singular and positive definite; otherwise, (26) degenerates [16] [17]. Taking into account this fact the CAV detector is useful to avoid such problems. As we have seen above that the CAV detector is a ratio between the sum of elements of the sample covariance matrix and the sum of diagonal elements of that matrix as:

$$\Lambda_{\mathrm{CAV}}(\mathbf{z}) = \frac{\sum_i^{NM} \sum_j^{NM} \mathrm{abs}\left(\lambda_{ij}\right)}{\sum_i^{NM} \mathrm{abs}\left(\lambda_{ii}\right)} \underset{\mathcal{H}_0}{\overset{\mathcal{H}_1}{\lessgtr}} \gamma, \tag{27}$$

here abs (.) is for absolute value, whereas λ_{ij} is the i, jth element of sample covariance matrix $\hat{\boldsymbol{\Sigma}}_{z,1}$. Test statistics (27) is not optimal like GLRT, but has robustness against the high-dimensionality effects in small sample support.

3.5 Experimental Results

Let us compare the performance of the traditional time-domain detectors exploiting both spatiotemporal correlations [3] with the proposed t–f-based detectors. In order to numerically analyze these schemes, we assume that the following signal is received by $m = 3$ sensors.

$$s = e^{2\pi j(an+bn^3)}, \tag{28}$$

where $a = 0.5$ and $b = 1.2207e-05$. The given signal is corrupted with white Gaussian noise with uncertain noise power, where noise power uncertainty is modeled using Eq. (17). ROC curves illustrating the performance comparison between traditional multi-sensor spatiotemporal detectors based on GLRT and CAV [3] and their t–f counterparts are shown in Figs. 8 and 9. Table 2 shows the area under the

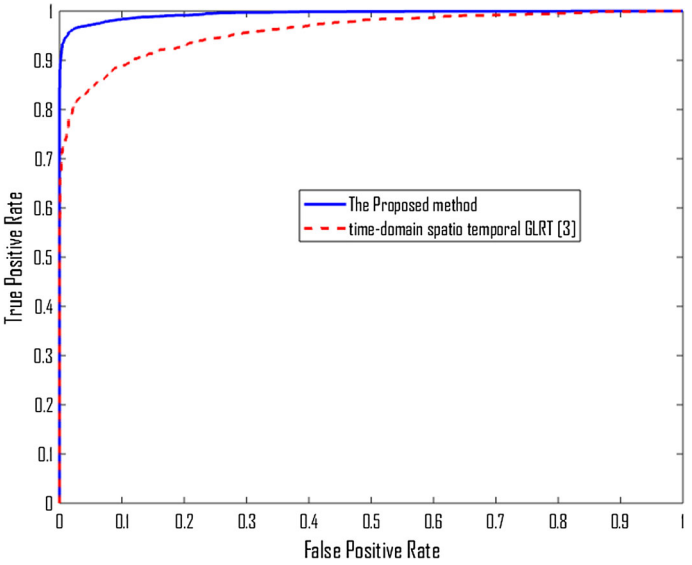

Fig. 8 Performance comparison with ROC between the proposed $t-f$ spatiotemporal GLRT detector versus traditional spatiotemporal GLRT detector [3]. Noise power uncertainty parameter $\alpha_{nu} = 2$

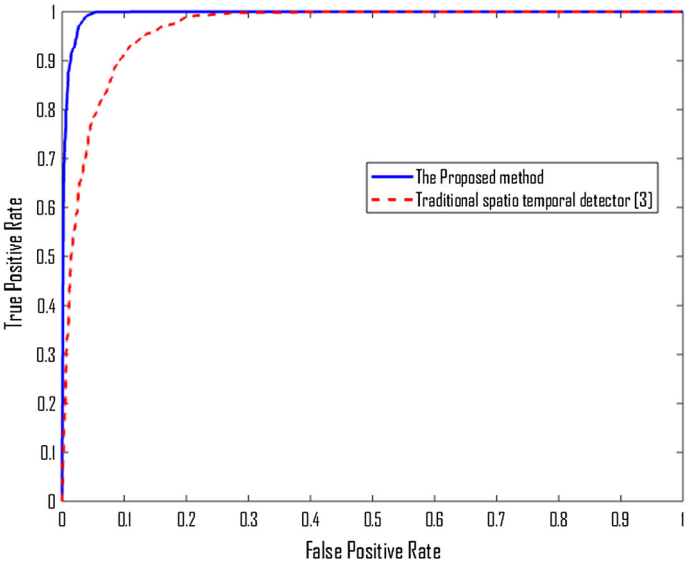

Fig. 9 Performance comparison with ROC curve between the proposed $t-f$ spatiotemporal CAV detector versus traditional spatiotemporal CAV detector [3]. Noise power uncertainty parameter $\alpha_{nu} = 2$

ROC curves of the two detection schemes. Experimental results indicate that the $t-f$ detection scheme performs better than the corresponding traditional time-domain detector.

Table 2 Area under ROC curve of the proposed $t-f$ detectors ($t-f$ CAV detector; $t-f$ GLRT detector versus conventional CAV detector [3] and GLRT detector [3])

$t-f$ CAV detector	CAV detector [3]	$t-f$ GLRT detector	GLRT detector [3]
0.9952	0.9653	0.9946	0.9593

Noise power uncertainty parameter $\alpha_{nu} = 2$

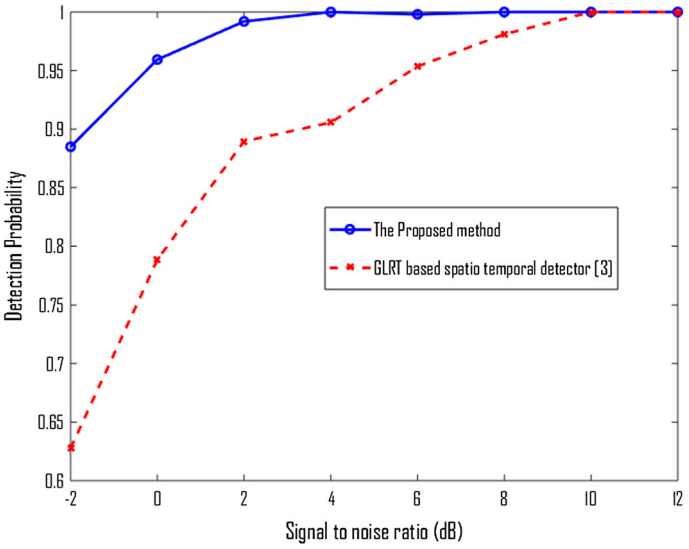

Fig. 10 Performance comparison between the proposed $t-f$-based spatiotemporal GLRT detector versus traditional spatiotemporal GLRT detector [3] using probability of detection at a false alarm rate of 1% plotted for different SNRs. Noise power uncertainty parameter $\alpha_{nu} = 2$

For further analysis of the above-mentioned schemes we plot probability of detection at a false alarm rate of 1% versus SNR. To compare the performance of the proposed $t-f$ schemes with the traditional schemes, we perform ROC analysis. The ROC curves for GLRT- and CAV-based detectors are shown in Figs. 10 and 11, respectively. These plots confirm the superiority of the proposed schemes over the traditional schemes because of their ability to exploit both spatial and temporal correlations, whereas the time-domain approach fails to exploit temporal correlation due to non-stationary characteristics of frequency-modulated signals.

Furthermore, we can also observe that in multi-sensor and mono-sensor cases, CAV detectors ($t-f$ and time domain) perform similar to GLRT detectors ($t-f$ and time domain) as both exploit correlations in addition to energy of the received signals though, asymptotically, GLRT is proven to outperform the CAV detector [3].

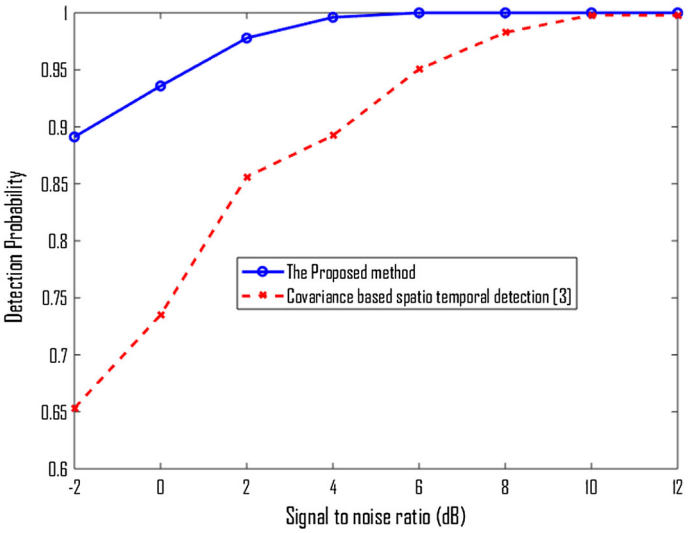

Fig. 11 Performance comparison between the proposed $t-f$ spatiotemporal CAV detector versus traditional spatiotemporal CAV detector [3] using probability of detection at a false alarm rate of 1% plotted for different SNRs. Noise power uncertainty parameter $\alpha_{nu} = 2$

4 Conclusion

A $t-f$ approach to signal detection has been developed for both mono-sensor and multi-sensor recordings. The proposed approach uses instantaneous frequency estimation and de-chirping procedure to remove frequency modulation, thus resulting in temporally correlated stationary signal. Experimental results demonstrate the superiority of the proposed method over existing techniques such as time-domain covariance-based signal detection method and energy detector. The proposed method has been developed aiming at the scenarios when there is an uncertainty in the noise power. The improvement in performance comes at the expense of increased computational cost of the proposed algorithm that requires the additional computations for obtaining a QTFD. The computational cost of computing a QTFD is $O(KN^2 \log N)$, where N is number of samples in a given signal and K is number of sensors employed. The proposed method has been developed for mono-component signals. However, it can be applied to multi-component signals as well. For multi-component signals, the method would require the IF estimation of the strongest component followed by de-chirping. The IF of the strongest component can be estimated by robust IF estimation algorithm given in [24]. This topic will be further explored in a future study.

References

1. S. Ali, J.A. Lopez-Salcedo, G. Seco-Granados, Improved GLRT based on the exploitation of spatial correlation between neighbouring sensors, in *Proceedings of 19th EUSIPCO*, pp. 1045–1049 (2011)
2. S. Ali, G. Seco-Granados, J.A. Lopez-Salcedo, Spectrum sensing with spatial signatures in the presence of noise uncertainty and shadowing. EURASIP J. Wirel. Commun. Netw. **2013**, 150 (2013)

3. S. Ali, D. Ramírez, M. Jansson, G. Seco-Granados, J.A. López-Salcedo, Multi-antenna spectrum sensing by exploiting spatio-temporal correlation. EURASIP J. Adv. Signal Process. **2014**(1), 1–16 (2014)
4. T.W. Anderson, *An Introduction to Multivariate Statistical Analysis*, vol. 2, 2nd edn. (Wiley, New York, 2003)
5. W.G. Anderson, R. Balasubramanian, Time-frequency detection of gravitational waves. Phys. Rev. D **60**(10), 102001 (1999)
6. E. Axell, G. Leus, E.G. Larsson, H.V. Poor, Spectrum sensing for cognitive radio: state-of-the-art and recent advances. IEEE Signal Process. Mag. **29**(3), 101–116 (2012)
7. B. Barkat, B. Boashash, A high-resolution quadratic time-frequency distribution for multicomponent signals analysis. IEEE Trans. Signal Process. **49**(10), 2232–2239 (2001)
8. B. Boashash, Estimating and interpreting the instantaneous frequency of a signal. II. Algorithms and applications. Proc. IEEE **80**(4), 540–568 (1992)
9. B. Boashash, G. Azemi, A review of time–frequency matched filter design with application to seizure detection in multichannel newborn EEG. Digit. Signal Process. **28**, 28–38 (2014)
10. B. Boashash, V. Sucic, Resolution measure criteria for the objective assessment of the performance of quadratic time–frequency distributions. IEEE Trans. Signal Process. **51**(5), 1253–1263 (2003)
11. S. Chen, X. Dong, Z. Peng, W. Zhang, G. Meng, Nonlinear chirp mode decomposition: a variational method. IEEE Trans. Signal Process. **65**(22), 6024–6037 (2017)
12. I. Djurović, A WD-RANSAC instantaneous frequency estimator. IEEE Signal Process. Lett. **23**(5), 757–761 (2016)
13. I. Djurovic, QML-RANSAC: PPS and FM signals estimation in heavy noise environments. Signal Process. **130**(Supplement C), 142–151 (2017)
14. S.S. Haykin, J. Litva, T.J. Shepher, *Radar Array Processing* (Springer, New York, 1993)
15. N.A. Khan, M. Sandsten, Time–frequency image enhancement based on interference suppression in Wigner–Ville distribution. Signal Process. **127**, 80–85 (2016)
16. O. Ledoit, M. Wolf, Some hypothesis tests for the covariance matrix when the dimension is large compared to the sample size. Ann. Stat. **30**(4), 1081–1102 (2002)
17. N. Lu, D.L. Zimmerman, The likelihood ratio test for a separable covariance matrix. Stat. Probab. Lett. **73**(5), 449–457 (2005)
18. S. Meignen, D.-H. Pham, S. McLaughlin, On demodulation, ridge detection, and synchrosqueezing for multicomponent signals. IEEE Trans. Signal Process. **65**(8), 2093–2103 (2017)
19. M. Mohammadi, A.A. Pouyan, N.A. Khan, A highly adaptive directional time–frequency distribution. Signal Image Video Process. **10**(7), 1369–1376 (2016)
20. J.M. O'Toole, B. Boashash, Time-frequency detection of slowly varying periodic signals with harmonics: methods and performance evaluation. EURASIP J. Adv. Signal Process. **2011**(1), 193797 (2011)
21. S.J. Shellhammer, S. Shankar, R. Tandra, J. Tomcik, Performance of power detector sensors of DTV signals in IEEE 802.22 WRANs, in *Proceedings of 1st International Workshop on Technology and policy for accessing spectrum (TAPAS)*, pp. 4–13 (2006)
22. P.-L. Shui, Z. Bao, S. Hong-Tao, Nonparametric detection of FM signals using time–frequency ridge energy. IEEE Trans. Signal Process. **56**(5), 1749–1760 (2008)
23. J. Simmons, Echolocation in bats: signal processing of echoes for target range. Science **171**(974), 925–928 (1971)
24. L.J. Stankovic, I. Djurovic, A. Ohsumi, H. Ijima, Instantaneous frequency estimation by using Wigner distribution and Viterbi algorithm, in *2003 IEEE International Conference on Acoustics, Speech, and Signal Processing, 2003. Proceedings.(ICASSP'03)*, Vol. 6. IEEE, pp. VI–121 (2003)
25. R. Tandra, A. Sahai, SNR walls for signal detection. IEEE J. Sel. Top. Signal Process. **2**(1), 17–24 (2008)
26. E. Visotsky, S. Kuffner, R. Peterson, On collaborative detection of TV transmissions in support of dynamic spectrum sharing, in *Proceedings of 1st IEEE DySPAN*, pp. 338–345 (2005)
27. S. Wang, X. Chen, G. Cai, B. Chen, X. Li, Z. He, Matching demodulation transform and synchrosqueezing in time–frequency analysis. IEEE Trans. Signal Process. **62**(1), 69–84 (2014)
28. W. Yang, G. Durisiand, V.I. Morgenshtern, E. Riegler, Capacity pre-log of SIMO correlated block-fading channels, in *8th International Symposium Wireless Communication Systems (ISWCS)*, pp. 869–873 (2011)

29. Y. Yang, X. Dong, Z. Peng, W. Zhang, G. Meng, Component extraction for non-stationary multi-component signal using parameterized de-chirping and band-pass filter. IEEE Signal Process. Lett. **22**(9), 1373–1377 (2015)
30. Y. Zeng, Y.C. Liang, Eigenvalue-based spectrum sensing algorithms for cognitive radio. IEEE Trans. Commun. **57**(6), 1784–1793 (2009)
31. Y. Zeng, Y.-C. Liang, Spectrum-sensing algorithms for cognitive radio based on statistical covariances. IEEE Trans. Veh. Technol. **58**(4), 1804–1815 (2009)
32. Y. Zeng, Y.-C. Liang, A.T. Hoang, R. Zhang, A review on spectrum sensing for cognitive radio: challenges and solutions. EURASIP J. Adv. Signal Process. **2010**, 381465 (2010). https://doi.org/10.1155/2010/381465